Materials Science & Engineering A 702 (2017) 173–183

Contents lists available at ScienceDirect

Materials Science & Engineering A

journal homepage: www.elsevier.com/locate/msea

Phase stability dependence of deformation mode correlated mechanical properties and elastic properties in Ti-Nb gum metal

Sumin Shin[a], Cheng Zhang[a], Kenneth S. Vecchio[a,b,*]

[a] Materials Science & Engineering Program, University of California, San Diego, La Jolla, CA 92093-0448, United States
[b] Department of NanoEngineering, University of California, San Diego, La Jolla, CA 92093-0448, United States

ARTICLE INFO

Keywords:
Gum Metal
β phase stability
Metastable titanium alloy
Mechanical twining
Stress-induced martensitic transformation

ABSTRACT

The evolution of microstructure and deformation modes in metastable Ti-23Nb-0.7Ta-2Zr-0.8O (at%) alloys with accumulated strain to 0.15 are investigated, where different solution treatments were applied to control both elemental distributions and the bcc β-phase stability. Recent studies suggest that the occurrence of specific deformation mechanism of the β-phase is strongly linked with its chemical stability. In the present study, the Bo-Md phase stability diagram was used to evaluate the β-phase stability and to discuss the deformation modes as function of solution treatment conditions, resulting in different deformed microstructures. Analysis of the deformed microstructure using electron backscatter diffraction and X-ray diffraction revealed that deformation bands formed at the initial stage of strain were composed of not only mechanically induced $\{332\}<112>_{\beta}$ and $\{112\}<111>_{\beta}$ twinning, but also stress-induced martensite α″ phase. It was observed that the number of deformation bands decreases with increasing homogeneity in the alloy, which is strongly dependent on the phase constitution, and directly impacts its final properties including hardness and elastic modulus. Based on the experimentally observed results, the β-phase stability dependence of deformation features can explain the possibility of manipulating the mechanical properties without the evident elastic properties variation in Ti-Nb Gum Metal.

1. Introduction

In recent years, there has been growing interest in materials science and industrial fields for multifunctional β-phase Ti alloys due to a good combination of elastic properties and mechanical properties [1–3]. Metastable β-Ti alloys, which can be defined as the least stable β-phase titanium alloys, have been developed to open a new possibility to expand the material property window between lower elastic modulus and better formability compared with conventional α, α + β, and β-phase Ti alloys [4–8]. With progress in developing multifunctional β-Ti alloys, tailoring the chemical stability of the β-phase has been an essential approach, which is strongly dependent on chemical composition of the alloys [9–11].

Gum Metals are the most well-known metastable β-phase Ti alloy, developed by controlling chemical composition [12], which fundamentally consist of Ti + [Nb or V] + Ta + [Zr or Hf] elements and oxygen. It is well documented in the literature [12–14] that these alloys possess “super-properties” such as low elastic modulus with high strength, and high ductility accompanied by little or no work hardening during cold working. These combinations of properties are rarely present in a single alloy. For these unique characteristics of the alloys, three critical electronic parameters are simultaneously satisfied [12]; (a) an average valence electron/atom ratio e/a ~ 4.24; (b) a bond order (Bo-value) ~ 2.87, and (c) d-electron orbital energy level (Md-value) ~2.45 eV. Furthermore, oxygen, with a range from 0.7 to 2.0 at%, is an essential element in the chemical composition [12]. The specific composition required for Gum Metal’s unique properties suggests that the characteristics of the alloys strongly correlate with their β-phase stability. Moreover, exceptional physical properties, such as nonlinear elastic behavior with an extended elastic limit, Invar-like thermal expansion, and Elinvar-like thermal dependence of the elastic modulus, can be achieved only after a certain amount of cold deformation [12]. This implies that the chemical composition of Gum Metal is not only related to the β-phase stability, but also to plasticity, which is considered as the most important factor to determine its characteristics. Plastic deformation of the Gum metal in processing is necessary to realize their unique properties.

Accordingly, there have been extensive studies investigating the deformation mechanism of Gum Metals to elucidate plastic deformation behavior [15–20]. Saito *et al.* [12,19–21] reported that the above

* Corresponding author at: Department of NanoEngineering, University of California, San Diego, La Jolla, CA 92093-0448, United States.
E-mail address: kvecchio@ucsd.edu (K.S. Vecchio).

http://dx.doi.org/10.1016/j.msea.2017.06.099
Received 14 May 2017; Received in revised form 24 June 2017; Accepted 27 June 2017
Available online 08 July 2017
0921-5093/

unique properties are attributed to a dislocation-free deformation mechanism, which is characterized by a distorted lattice containing nanodisturbances (referred to as "giant faults"). It supported in the literature [22,23] that the ideal strength of Gum Metal is achieved by means of a non-conventional plasticity mechanism, accommodated by with low resistance to shear along certain crystallographic planes, where the trigger stress for bulk shear is smaller than the critical resolved shear stress to move dislocation on their slip planes. However, several studies have recently shown that conventional deformation mechanisms are operative during plastic deformation in Gum Metals [16,17,22–27]. For example, mechanically induced twinning [17,23] and stress-induced phase transformation [16,22,23] have been reported to be active in a deformed typical Gum Metal, Ti-23Nb-0.7Ta-2.0Zr-1.2O (at%) alloy. In addition, Yang et al. observed dislocation glide on slip planes with increased oxygen content in Ti-22.4Nb-0.73Ta-2.0Zr-1.34O (at%), whose β phase stability is slightly higher than that of nominal Gum Metal [16,24–27]. Oxygen is considered a β stabilizing element in metastable β alloys [12,26]. Therefore, these results imply that not only are multiple deformation mechanisms activated in Gum Metals, but also the main mechanism operative can be controlled by the β-phase stability.

It was found that the deformation behavior of metastable β-Ti alloys is closely related to the β-phase stability [9,10,13,28–30], characterized by the ability to transform into martensite phase by cooling or external stress [31]. As discussed in the literature [10,27,28], deformation in stable β-Ti alloys is mainly accompanied by dislocation slip, while the activated deformation modes are changed with decreasing the β-phase stability, including mechanically-induced $\{332\}<113>$ twinning, $\{112\}<111>$ twinning, or stress-induced α'' martensitic transformation [15–17,30]. It has also been observed that multiple deformation mechanisms can co-exist, which results in a complex deformation behavior of metastable β-Ti alloys [16,24,30–32]. To establish the relationship between plastic deformation behavior and β-phase stability, two-dimensional phase stability diagrams have very recently been applied [31–34], utilizing the electronic parameters: bond order (Bo) and d-orbital energy level (Md). Morinaga et al. [35,36] suggested that the two electronic parameters (Bo and Md) connect with the relative chemical stability of the β phase, where Bo is the covalent bond strength between Ti and each alloying elements, and Md represents the electronegativity. These values were calculated using the following equations [35]:

$$\overline{Bo} = \sum_{i=1}^{n} xi(Bo)i \quad (1)$$

$$\overline{Md} = \sum_{i=1}^{n} xi(Md)i \quad (2)$$

Here, xi is the atomic fraction of an alloying element and $(Bo)i$ and $(Md)i$ are the Bond order values and metal d-orbital energy level for element i, respectively. Furthermore, this phase stability map provided correlation of the chemical stability of the β-phase with the occurrence of the dominant deformation mechanism using experimental data from a wide variety of alloying system [35], which is experimentally corresponding to the preferred activation of mechanically-induced twinning, stress-induced martensitic transformation and dislocation slip [30,31]. The Bo-Md phase stability diagram is therefore a very useful tool for investigating how plastic deformation behavior is affected by alloy composition that corresponds the phase stability of β-Ti alloys.

Compositional optimization has been widely used to achieve a superior combination of mechanical properties in metastable β-Ti alloys [12,33,37–39], because it is strongly linked with the presence of multiple phases that can be manipulated by materials processing and optimized alloy design. Based on this methodology, earlier reports [30,32–34] suggest that the various deformation modes operative in a given alloy play a crucial role in enhancing the work hardening rate, and thus significantly improving the poor ductility caused by strain localization in conventional slip-dominated β-Ti alloys. The improvement in mechanical properties is attributed to the simultaneous occurrence of TRansformation-Induced Plasticity (TRIP) effect and TWinning-Induced Plasticity (TWIP) effect [33,34]. As such, compositional optimization is considered an approach to potentially control microstructure and optimize mechanical properties in β-Ti alloy.

Given the remarkable effects of Gum metal's composition on its physical properties, it is surprising how few studies have examined this approach to control the mechanical properties of Ti-Nb Gum Metal. Therefore, this study is aimed to improve and/or control the mechanical properties of Gum metal through manipulating deformation behavior in association with the chemical stability of the β-Ti phase. Different solution treatments were employed to achieve various β-phase stabilities through homogenizing the elemental distributions in a metastable β, Ti-23Nb-2Zr-0.7Ta-0.8O (at%) alloy. The evolution of deformation mechanisms with respect to the β-phase stability is investigated, as well as discussion of the possibility of manipulating the mechanical properties without evident elastic modulus variation in this Ti-Nb Gum Metal.

2. Experimental

A master alloy with a nominal composition of Ti-23Nb-2Zr-0.7Ta-0.8O (at%) was produced using a mixture of pure elements Ti, Nb, Ta, Zr, and powder TiO_2. Owing to the difference in the melting point and density of raw materials, two kinds of ingots were first fabricated by arc-melting under argon atmosphere: i) Ti + Zr + TiO_2, and ii) Nb + Ta. After melting these two ingots separately, they were combined together by arc melting, also under argon atmosphere. The resulting ingot was melted at least five times to avoid in-homogeneity due to un-melted elements or a lack of molten mixing. To minimize elemental segregation adjacent to grain boundaries, the ingot was held in an inert-gas induction furnace for 30 min in its liquid state. The chemical composition of the as-cast alloy is listed in Table 1. In order to achieve different elemental distribution in each sample, the solution treatment was performed for 100, 1000 or 3000 min at 1273K (above the β transus) under vacuum followed by quenching into water. These solution-treated specimens are referred to hereafter as ST100, ST1000, and ST3000, respectively. The microstructure of the as-solution treated alloys consists of large equiaxed grains whose average size was ~1200 μm shown in Fig. 1(a), irrespective of the different solution treatment times used in this study. For investigating the evolution of the deformation microstructure with accumulated strain, the samples for cold rolling were prepared with the following dimensions: 35 mm in length, 10 mm in width and 10 mm in thickness. These samples, following the solution-treatment, were cold-rolled to a strain from 0.02 to 0.15, at room temperature. These cold-rolled samples were cut with a slow cutting speed to minimize any heating effects on the samples.

Specimens for structural investigations were first ground using SiC papers and then mechanically polished with 3 μm, 1 μm diamond, and 0.05 μm SiO_2 solutions. The polishing process was performed under a load of 5 N to avoid the formation of stress-induced α" martensite phase on the surface; no subsequent etching was applied. Electron backscattered diffraction (EBSD) and scanning electron microscopy (SEM) were carried out on the plane parallel and normal to the rolling direction (RD) using a Bruker e-Flash EBSD detector on a FEI Quanta 600 SEM at 20 kV. Scans for EBSD were performed with a step sizes between 0.5 and 1.0 μm and working distance around 20 mm. In order to determine the local misorientation of deformed structures, the Kernel

Table 1
Chemical composition of as-cast Ti-Nb-Ta-Zr-O alloy.

Element	Ti	Nb	Ta	Zr	O
at%	Balance	22.8	0.71	2.02	0.80
wt%	Balance	35.5	2.15	3.09	0.21

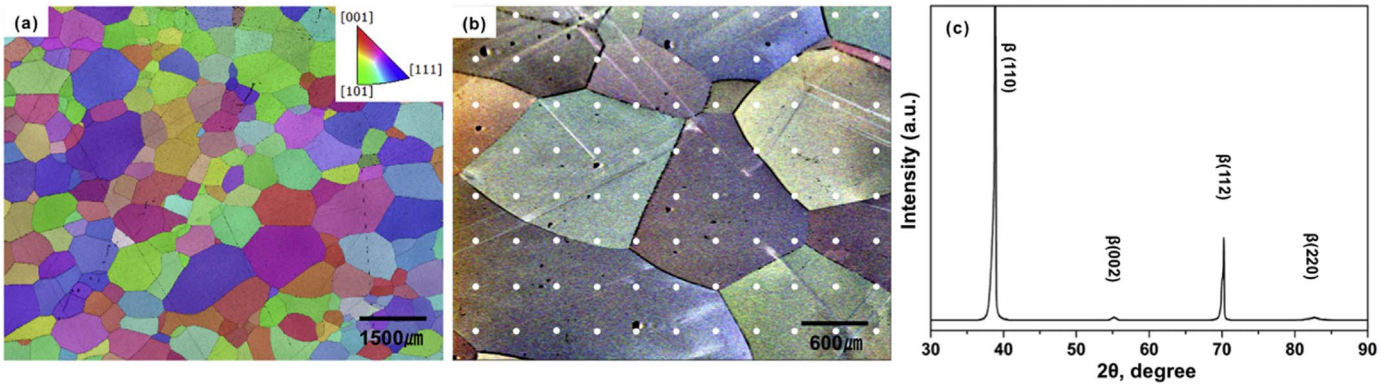

Fig. 1. (a), (b) Microstructure and (c) XRD pattern of the solution-treated alloy for 100 min (ST100). The white spots in (b) represent locations for EDS analysis depicted in Fig. 2a for the ST100 sample. Similar data point locations were selected for analysis of elemental compositions for samples ST1000 and ST3000 used in Fig. 2b and c, respectively.

averaged misorientation (KAM) analysis was applied with misorientation ranges from 0 to 5°. The element composition of the microstructure was measured quantitatively by energy dispersive spectroscopy (EDS) using point-spot analysis as show Fig. 1b. To identify phase structures, X-ray diffraction (XRD) was conducted with Cu Kα radiation. The body-centered cubic β phase was the only phase detected in the as-solution treated specimens shown in Fig. 1c.

Microhardness measurements were performed on the polished samples by Vickers hardness tester with a load of 1.0 kg. for 20 s. An average of the microhardness measurements was obtained from six indentations (the measured error was within 2%). The elastic modulus of the specimens was determined with acoustic wave-speed measurements obtained from ultrasonic sound speed and the material's density measured by Archimedes' principal. The measurements of wave speed and density of pure Ti (99.99 at%) was utilized for a calibration.

3. Results and discussion

3.1. Elemental distribution and phase stability

Fig. 2 shows the distributions of the elements Ti, Zr, Nb and Ta in the three samples obtained by different solution treatments (ST100, ST1000, and ST3000), where the composition of each element was determined by EDS analysis, at locations represented as dots in Fig. 1b. Both the ST100 sample (Fig. 2a) and the ST1000 sample (Fig. 2b) displayed significantly broader ranges of elemental distributions compared to that of the ST3000 sample. These EDS results were repeated several times on different locations in each sample. Table 2 presents the average compositions of Ti, Zr, Nb and Ta, and the variation of elemental distribution in the ST100, ST1000 and ST3000 samples. The results indicate that all samples have almost the same average values of each element in the as-solution treated samples. On the other hand, the difference between the maximum and minimum composition of Ti, Zr, Nb and Ta was 6.8%, 0.69%, 5.7% and 0.61%, respectively, in the ST100. The variation in composition of Ti, Zr, Nb and Ta in the ST1000 was 5.8%, 0.62%, 4.6% and 0.53%, respectively, showing a narrower range compared to that in the ST100. As shown in Fig. 2c, the ST3000 sample has a very small variation of elemental distributions, indicating that composition homogeneity was achieved by increasing the solutionizing time to 3000 min. Therefore, the EDS analysis indicates that both the ST100 and ST100 were clearly heterogeneous, which results from the sluggish diffusion of these refractory, β stabilizing elements

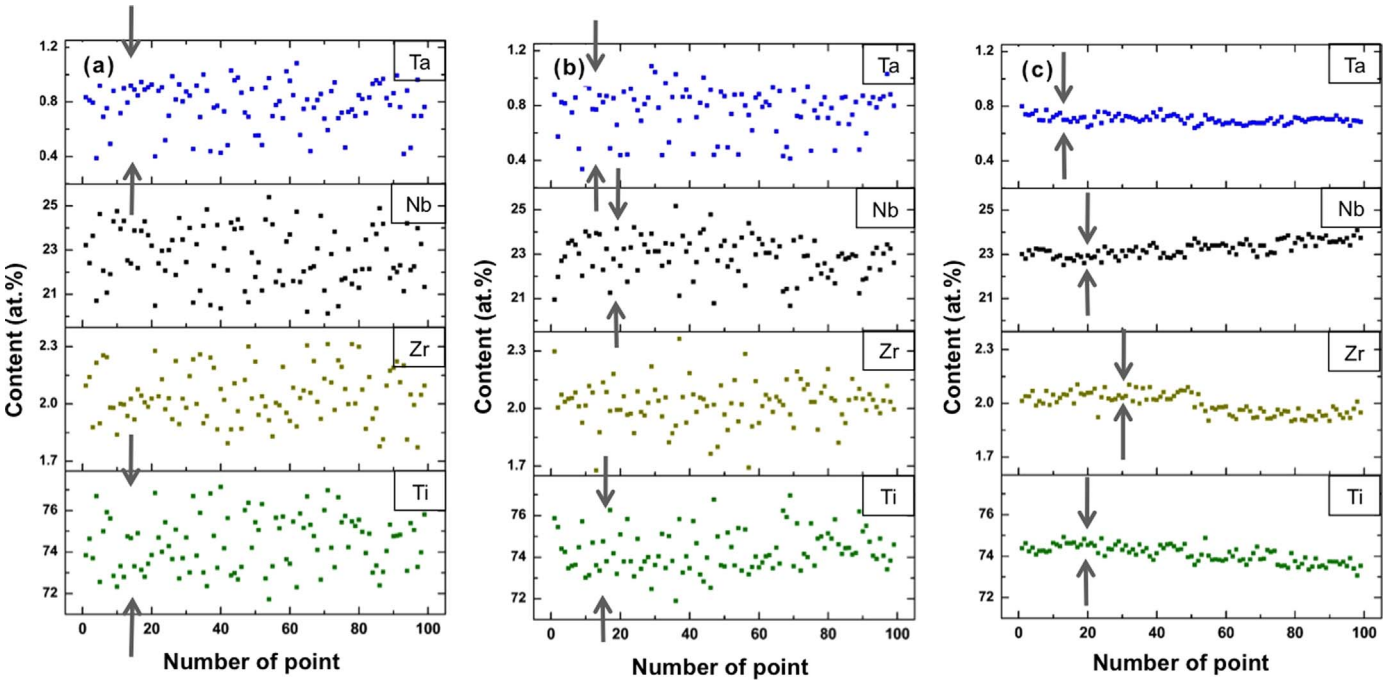

Fig. 2. Elemental distributions of Ti, Nb, Ta and Zr in samples of the same alloy melt, but solutionized for different times (a) ST100, (b) ST1000 and (c) ST3000. Arrows depict the elemental ranges within each plot.

Table 2
Measured contents of each element and calculated variation of elemental distribution in the ST100, ST1000 and ST3000 samples.

Samples	Ti		Zr		Nb		Ta	
	Average (at%)	Δcontent (at%)	Average (at%)	Δcontent (at%)	Average (at%)	Δcontent (at%)	Average (at%)	Δcontent (at%)
ST100	74.32	6.8	2.03	0.69	22.89	5.7	0.76	0.61
ST1000	74.45	5.8	2.05	0.62	22.72	4.6	0.78	0.53
ST3000	74.10	0.7	2.00	0.06	23.16	0.9	0.74	0.03

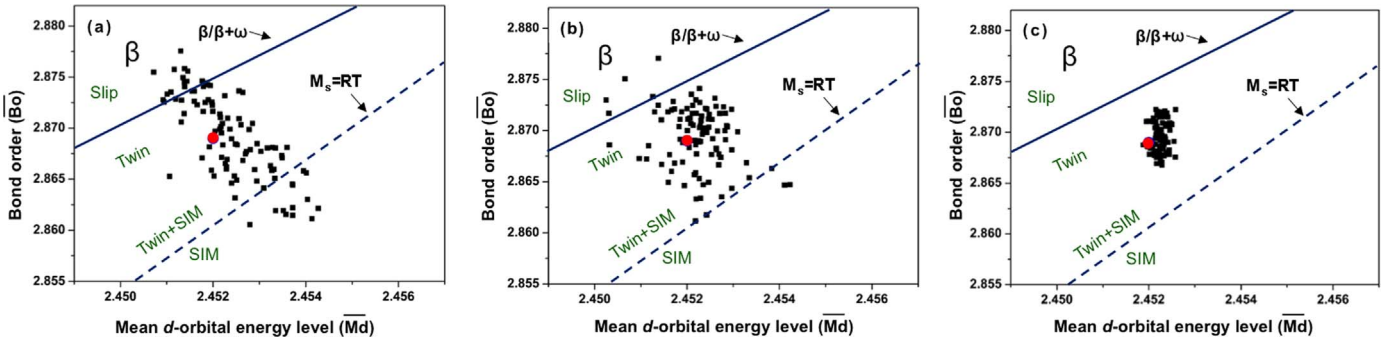

Fig. 3. β-stability as function of solution treatments: (a) ST100, (b) ST1000 and (c) ST3000. Each point superimposed on the $\overline{Bo}$-$\overline{Md}$ diagram corresponding to a specific EDS point-spot result shown in Fig. 2. The red point on the map represents the β-phase stability of the Ti-23Nb-0.7Ta-2.0Zr-1.2O (at%) overall alloy composition.

and insufficient solutionizing time, while a fully homogenized structure was achieved by increasing the solutionizing time to 3000 min for the ST3000 sample. Furthermore, this suggests that elemental distributions in Ti-Nb Gum metal can be controlled by the solution treatment process, which influences the β-phase stability of this alloy.

As shown in Fig. 3, the Bo-Md phase stability diagrams, derived from the work by Morinaga et al. [35], was adopted here to evaluate the β-phase stability of various microstructures in this study, where the β/β + ω phase boundary, represented by a solid line, indicates a region of the least stable single phase β. Martensite phases such as ω, α' or α″, depending on the alloy composition, could exist predominantly below the boundary for the martensite start temperature, for samples at room temperature (*Ms* = RT) as given by a dotted line in Fig. 3. It should be noted that the boundaries used for this diagram have been proposed by M. Abdel-Hady and coworkers [36], which showed some discrepancies with Morinaga's diagram [35,40]. As is mentioned by others [26,36], the addition of oxygen to metastable β-Ti alloys have been shown to suppress hexagonal ω phase formation upon quenching, and decreases the Ms transition temperature, illustrating that oxygen works as a β-phase stabilizer in Ti-Nb Gum Metal. Based on this observation and the results found in this study, it is thus reasonable to adopt modified boundaries for both the β/β + ω phase and the *Ms* transition, when considering the alloying effect of oxygen on the β-phase stability.

The composition data shown in Fig. 3 is derived from the EDS data (Fig. 2) and the Bo and MD values of alloying elements (Table 3), and indicates the β-phase stability variation in the alloys as function of solution treatments, where the alloying vectors (Bo and Md) were calculated for different locations within the microstructures. Position of each point, presented by the symbol ■ on the phase stability map, is related with the relative β-phase stability, which corresponds to the EDS point-spot results represented for example in Fig. 1b. In addition, the Bo-Md diagram indicated the preferred activation of deformation mechanisms with the β-phase stability [35,36]. The nominal composition of this Ti-Nb Gum Metal, with the values Bo = 2.869 and Md = 2.452, falls in the twinning region of Bo-Md map, as indicated by a red point in each part of Fig. 3. Accordingly, the predominant deformation mode activated in the alloy is expected to be mechanical twinning during the initial stages of deformation, which correspond well with experimental results reported by others [22–26,41,42]. On the one hand, the ST100 and ST1000 samples exhibit a wide region of β-phase stability from a region of stable β phase to a region of martensitic phase dominated, resulting from the heterogeneous elemental distributions. These results imply that the constituent β phase of these alloys possessed varying chemical stability, which is compositionally dependent. Previous reports [10,13,26,43] showed that the dominant deformation mechanism in metastable β-Ti alloys strongly rely on the β-phase stability, similar to the stacking fault energy in FCC metals. Based on existing theories and experimentally observed results, there is a strong possibility of multiple deformation mechanisms operative in these heterogeneous sample, rather than deformation by a single mechanism.

Table 3
List of the Bo and Md values for each of the alloying elements in bcc Ti [36].

Element	Ti	Nb	Ta	Zr
Bo	2.790	3.099	3.144	3.086
Md (eV)	2.477	2.424	2.531	2.934

With increasing solutionizing time, however, the data points (black squares) scatter decreases and converge toward the red circle data point (representing the bulk Ti-Nb Gum metal composition) shown in Fig. 3c. This implies that the β-phase stability in the ST3000 sample was more uniform, resulting from a more homogenized elemental distribution, as previously shown in Fig. 2c. This result suggests that one single deformation mechanism would be primarily operative in this alloy when its elemental distribution is fully homogeneous.

3.2. Phase stability dependence of deformation microstructures

Fig. 4 shows the representative microstructures of three samples after cold-rolling (ε = 0.02), which were observed using EBSD analysis. The crystallographic orientation is presented by inverse pole figure (IPF) coloring scheme as indicated in the inset in Fig. 4a, in which the observed plane is parallel to the rolling direction (RD). The same color scheme was applied to all of the orientation maps used in this study. The small amount of black in the IPF maps indicate areas with little or no indexed patterns, which may be due to difficulty in indexing SIM α″ with EBSD mapping. The observed microstructures show localized deformation bands formed in the equiaxed grains after plastic deformation. The IPF maps (Fig. 4a and b) for the ST100 and ST1000,

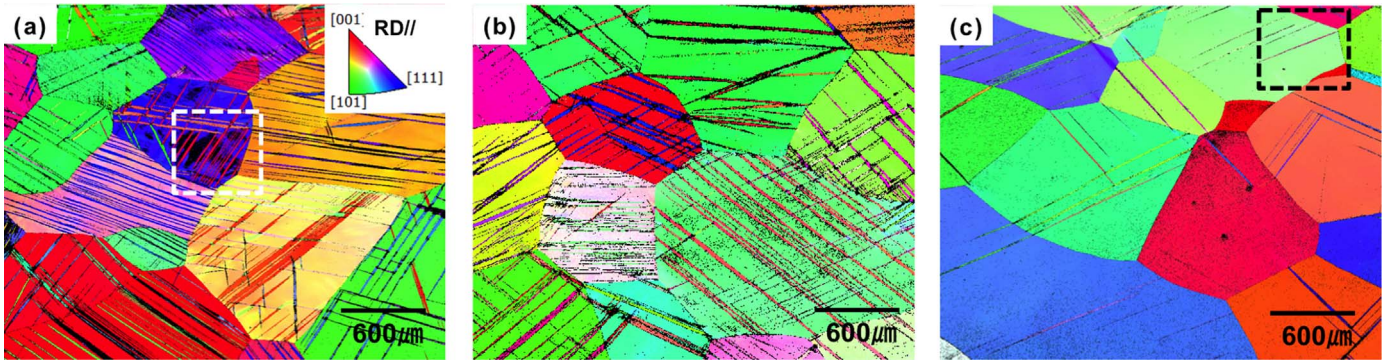

Fig. 4. Inverse pole figure maps of deformation microstructures in specimens with a strain of 0.02: (a) ST100, (b) ST1000, (c) ST3000. The observed plane is nominal to the rolling plane.

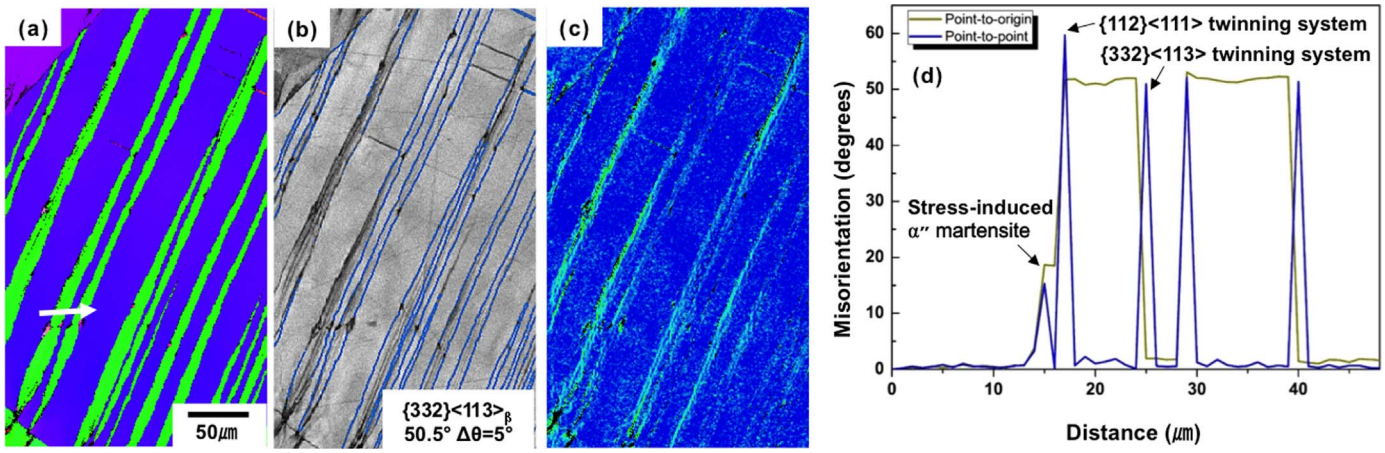

Fig. 5. EBSD analysis of deformation bands formed in the ST100, a heterogeneous structure: (a) IPF map, (b) IQ map superimposed with boundaries for {332} < 113 > twins delineated by the blue lines, (c) KAM map and (d) Misorientation profile along the arrow in (a).

respectively, depict similar microstructures that were composed of numerous plate-like features ~1 μm in size. The initiation of these deformation bands appears to start from one boundary and stopped at another grain boundary or by other band structures. These deformation bands do not propagate though grain boundaries to neighboring grains. It has been reported that the deformation bands in Ti-Nb Gum Metals result from primarily mechanical twinning [10,41,42]. However, it will be shown later that the bands can be composed of mechanical twinning or martensite α″ phase. On the other hand, Fig. 4c reveals that only a few deformation bands with parallel thin lines were observed in the ST3000 sample, illustrating that each sample deformed differently with the different solution treatment times (ST). The results in Fig. 4 indicate that the deformation bands in strained grains significantly decreased with increasing ST time, where the average number of the bands in a grain is about 25.8, 12.7 and 6.5 in the ST100, ST1000 and ST3000 samples, respectively. Clearly the extent of the deformation bands varies with the degree of compositional homogeneity, with longer solutionizing times and therefore greater homogeneity resulting in fewer deformation bands.

As discussed in the Section 3.1, the dominant deformation mechanism is dependent on the β-phase stability, which is strongly related to chemical composition of the alloys [9,10,13]. It is thus conceivable that deformation microstructure would significantly be influenced by the β-phase stability of the alloy. In particular, previous reports [29,39] found that the critical stress to trigger SIM (α″) decreased when the chemical composition was close to the Ms transition line, implying that the SIM transformation was easily activated by a small amount of external stress in the less stabilized β-Ti alloys. Therefore, it is essential to consider the β-phase stability in the specimens, to correlate to different fractions of deformation band in the microstructures. As shown in Fig. 3, the relatively lower β-phase stability was found in the ST100 and ST1000 samples, compared to that in the ST 3000 sample, can be correlated to a higher fraction of deformation bands in the microstructures. In addition, Min et al. [43] have reported that different level of homogeneity in β-Ti alloys led to various deformation features, especially enhancement of mechanical twinning rather than dislocation slip. This suggests that the existence of the heterogeneous elemental distribution results in the formation of low β-phase stability regions, which can be the nucleation site for mechanical twinning [34,43,44]. Consequently, the occurrence of a heterogeneous twin formation was attributed to a high fraction of the deformation bands in grains [43]. As shown in Fig. 4, similar to previous work [43], a heterogeneous elemental distribution led to a high fraction of the bands in the ST100 and ST1000 samples, demonstrating that the fraction of deformation bands in an early stage of deformation was highly dependent on elemental distributions.

3.3. Characteristics of deformation band

In order to identify the internal structure of the deformation band, ST100 and ST3000 samples were further characterized by EBSD analysis with the areas highlighted in Fig. 4a and c corresponding to ST100 and ST3000 samples, respectively. The IPF map (Fig. 5a) shows several intragranular bands, tens of micrometers in size, formed in the inhomogenized β matrix, with parallel thick laths induced by deformation. The deformation bands exhibit different color with that of the parent phase, which implies that their crystallographic orientations differ from each other. Fig. 5b shows that most of the bands were indexed as {332} < 113 > $_\beta$ (indicated with blue lines) that corresponds to the crystallographic misorientation of 50.5° between the β-matrix and {332} < 113 > $_\beta$ twin along the < 110 > $_\beta$ direction [45]. These observations indicate that the deformation structures are twin bands.

However, some part of bands was not delineated as {332} < 113 > $_\beta$ on the image quality (IQ) map, especially in the dark color area shown in the Fig. 5b. It is worth noting that the image quality map reflects lattice distortion in accordance with lattice imperfection [46]. Hence, dark contrast in the bands indicates higher lattice distortion, which means that the band was not purely composed of only {332} < 113 > $_\beta$ deformation twins. To characterize the deformation bands in more detail, the local lattice distortion was analyzed by the Kernel average misorientation (KAM) as shown in Fig. 5c, where the KAM values represent the density of geometrically necessary dislocation (GND) [47,48]. Observation of darker regions in the image quality map (Fig. 5b) correspond higher KAM values. This suggests there are additional deformation mechanisms operative beyond the {332} < 112 > $_\beta$ twins during deformation. Fig. 5d shows the point-to-origin and point-to-point misorientation profile along the arrow, presented in Fig. 5a, illustrating the strain was mainly activated by multiple deformation modes. This figure shows that stress-induced martensite (SIM) α″ was formed along the distance between 12 μm and 16 μm, corresponding to the point-to-point misorientation of 15.6°. The corresponding point-to-point misorientation of 59.9° was identified as {112} < 111 > twins [45], while {332} < 113 > twinning was defined with the characteristic 50.9° point-to point misorientation angle, as shown in Fig. 5d. Superimposing the misorientation and twin boundaries onto the IQ map, reveals that the deformation band was composed of α" / {112} < 111 > $_\beta$ twin / {332} < 113 > $_\beta$ twin / β matrix in sequence. Therefore, these images shown in Fig. 5 indicate that the strain in the in-homogenized sample was accommodated by multiple deformation mechanism, including stress-induced martensitic transformation and mechanically induced twins during the early stages of deformation.

Fig. 6 shows EBSD analysis of the deformation bands formed in ST3000, corresponding to a homogeneous elemental distribution in the specimen. These images illustrate that, in the homogenized β matrix, mechanical twinning was the only mechanism activated at a strain of 0.02. In the image quality map (Fig. 6b), the bands were fully indexed as {332} < 113 > $_\beta$, where the image contrast color of the whole deformation band is nearly the same along its entire length. In addition, no obvious additional misorientations with the β matrix were observed by the KAM analysis as shown in Fig. 6c. In addition, the misorientation profile (Fig. 6d) clearly shows that {332} < 113 > $_\beta$ mechanical twinning was solely activated as the deformation mechanism. This suggests that Ti-Nb Gum metal, when compositionally homogeneous, deforms by mechanical twinning at the initial stages of strain.

Based on the above results, the operative deformation mode was obviously different between the ST100 and ST3000 samples, even with the same bulk chemical composition. According to previous studies [10,32,49,50], the deformation mechanisms in metastable β titanium alloys strongly rely on the matrix conditions such as grain orientation, grain size and phase stability, and should be considered. In the present study, all samples, even with different solution treatments, were shown to have essentially the same grain size, and possessed no obvious texture, as presented in Fig. 4. Hence, it is reasonable to consider only the phase stability affecting the deformation mechanism in the alloys. Recall that a single master alloy was cast from which all the different solutionizing samples were created. Lai *et al.* [48] reported that the deformation behavior was accompanied by multiple deformation mechanisms in Ti-23 Nb-0.7Ta-2.0Zr (at%) with no oxygen included, an alloy with lower β-phase stability than a nominal composition of Gum Metal (since oxygen works as β stabilizer by retarding ω phase formation). It was found that the deformation bands formed in the less stable β-Ti alloys were composed of {332} < 113 > $_\beta$ twinning, {112} < 111 > $_\beta$ twinning and SIM α″, in good agreement with our results obtained from the ST100 sample, as shown in Fig. 5. It suggests that the deformation bands formed in a compositionally heterogeneous sample was attributed to the relatively lower β-phase stability, which was mainly observed in the ST100 deformed at a strain of 0.02. On the other hand, it is found by others [22,51] that Gum metal undergoes a reversible stress-induced martensitic phase transformation (α″→β) during the unloading process at the initial stage of strain. The above result demonstrated that mechanical twinning was the primary deformation mechanism in Ti-25 Nb-0.7Ta-2Zr-1.2O (at%) alloy, which is well supported by the deformation bands formed in the ST3000 sample. This study thus highlights the fact that the deformation behavior of Ti-Nb Gum metals is closely related to the β-phase stability that can be controlled by alloying element distributions as shown in Fig. 3.

3.4. Effect of β-phase stability on deformation mechanism

To investigate the effect of chemical stability on the deformation behavior, the microstructure of individual grains in the ST1000 sample were observed after cold-rolled to 5% reduction (ε = 0.05). Fig. 7a-c shows the typical deformation microstructures corresponding to the β-phase stability (Fig. 7d) in the deformed ST1000. Clearly different deformation features, with different fractions of parallel thin bands and thick lathes, were revealed in strained grains (Fig. 7a-c). This implies that the deformation behavior was accompanied by different plastic deformation mechanisms in β-grains. It should be state that deformation bands nucleated at one grain boundary and propagated either to the middle of the grain intersecting with other bands or terminated at another grain boundary. Hence, the deformation mode occurring in one grain has little or no influence on the deformation mechanisms of neighboring grains. In the micrograph of grain A, shown in Fig. 7a, a few deformation bands 0.1–1.5 μm in width were observed. As

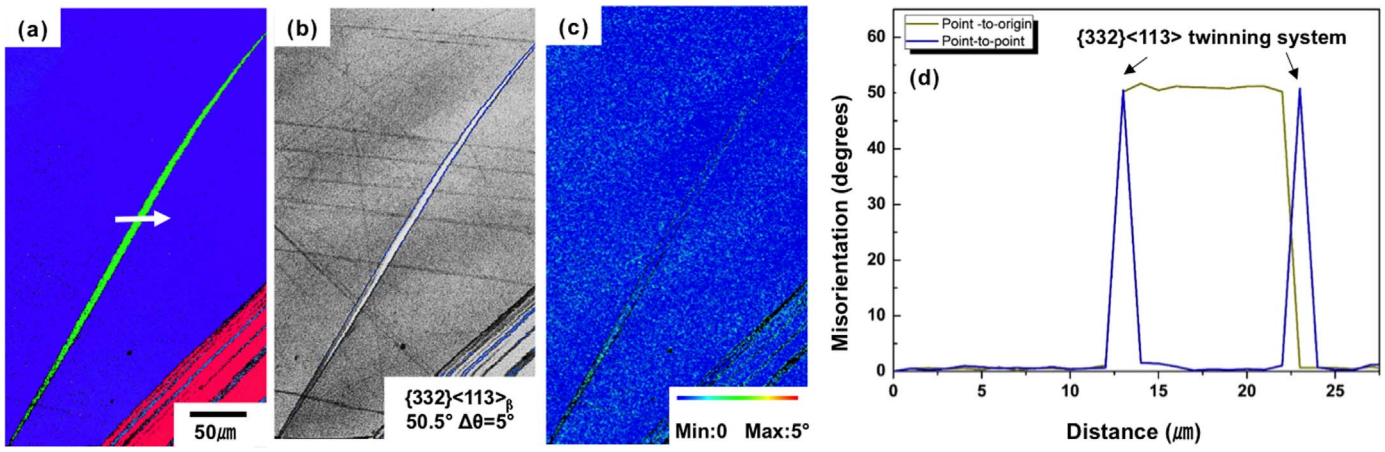

Fig. 6. EBSD analysis of deformation band formed in the ST3000, a fully homogenized structure: (a) IPF map, (b) IQ map superimposed with boundaries for {332} < 113 > twins delineated by the blue lines, (c) KAM map and (d) Misorientation profile along the arrow in (a).

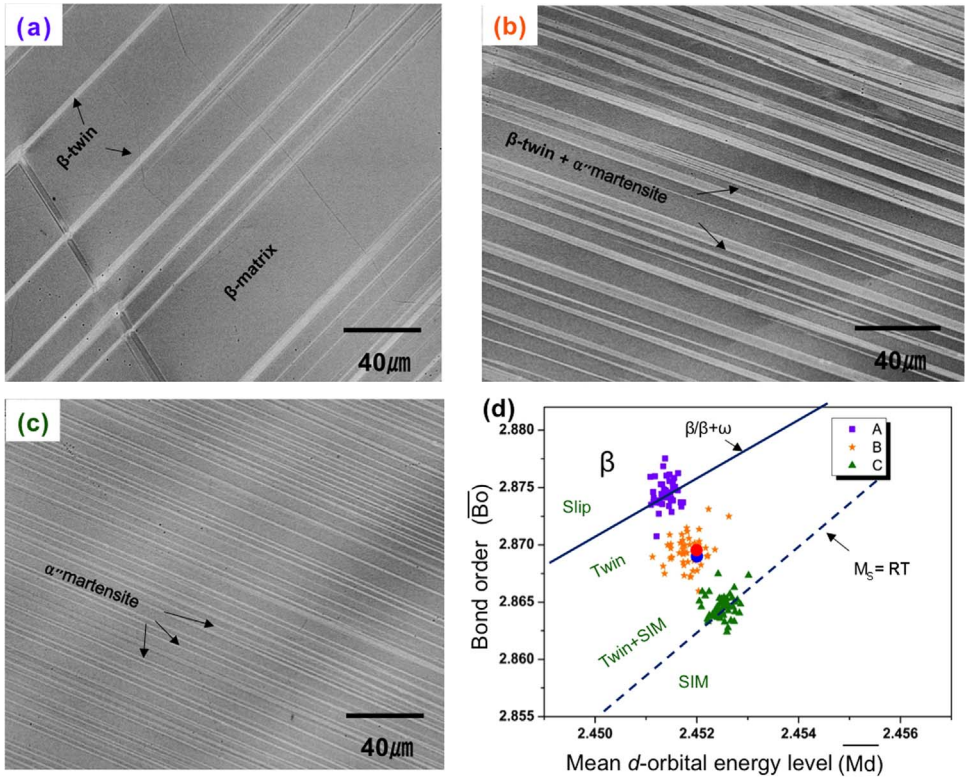

Fig. 7. (a, b and c) SEM images of the ST1000 subject to 5% cold rolling (ε = 0.05), (d) β-phase stability relative to the Grain A (a), Grain B (b), and Grain C (c) superimposed on the $\overline{Bo}$ - $\overline{Md}$ diagram. The red point on the map represents the β-phase stability of a Ti-23Nb-0.7Ta-2.0Zr-1.2O (at%) alloy.

described in the previous section, the thick-lath features were characteristic of mechanical twinning, and the thin bands were considered to be stress induced martensite (SIM, α"). In grain B, shown in Fig. 7b, the numbers of bands significantly increased and were thicker compared to grain A. It is clear that the bands formed in the grain B are comprised of both mechanical twins and SIM (α"), as indicated in Fig. 7b. Finer band features of the microstructure were observed in Fig. 7c, corresponding to grain C, and no thick laths were present. The observed thin bands were identified by SIM α″ with 5–20 nm in width, indicating that the occurrence of stress-induced martensite α″ transformation led to a dense network of nanoscale thin band structures [52]. These observations (Fig. 7a-c) demonstrate that different β grains respond to plastic behavior in different way in a heterogeneous specimen. Composition differences between grains directly alter the deformation mode of individual grains.

Fig. 7d displays the β-phase stability of each grain, corresponding to the grain A (Fig. 7a), the grain B (Fig. 7b) and the grain C (Fig. 7c), on the $\overline{Bo}$ - $\overline{Md}$ diagram, where the Bo and Md values of individual grains were calculated as described in Section 3.1. The obtained β-phase stabilities in three grains were obviously different due to a heterogeneous elemental distribution shown in Fig. 3b, which can lead to various deformation mechanisms. The corresponding β-phase stability in grain A shows most points were located near or above the β/β + ω-phase boundary (i.e. in the stable β-phase region), illustrating that plastic deformation in this grain was mainly accommodated by mechanical twins or dislocation glide on slip planes, which is in close agreement with the micrograph of grain A. Furthermore, the relatively stable β-phase was strongly correlated with a small number of visible deformation bands in grain A. On the other hand, lower stability of the β-phase was revealed in grain B, where composition measurements yield $\overline{Bo}$ - $\overline{Md}$ values that mostly fall in the area between the β/β + ω-phase boundary and the Ms transition line. Observation of the microstructure indicates characteristics of mechanical twins and SIM (α″), with a high number of deformation bands within grain B, as shown in Fig. 7b. In the $\overline{Bo}$ - $\overline{Md}$ diagram, the β-phase stability obtained from grain C was mainly located near the Ms transition line, where the SIM α″ transformation was predominantly taking place during plastic deformation, as was pointed out in Section 3.2. These observations indicate that the preferential activation of a deformation mechanism in different β-grains is closely linked to the chemical stability of the β-phase. In addition, it also plays a significant role in determining deformation behavior of the alloy as a whole, as different deformation mechanisms lead to different levels of ductility and homogeneity of deformation.

3.5. Effect of phase stability on phase constitution in cold-rolled alloys

Fig. 8 presents IPF maps of typical microstructures observed in the ST100 (Fig. 8a and c) and ST3000 (Fig. 8b and d) specimens after cold rolling to 15% reduction (ε = 0.15). In a general view of the deformed microstructures shown in Fig. 8a and b, there were obvious changes in the band number and their volume fractions between an in-homogenized specimen (ST100) and a homogenized specimen (ST3000). As mentioned in Section 3.2, this is likely a result of differences in the elemental distributions between the ST100 and the ST3000 samples. In the IPF map of the ST100 sample, at a strain of 0.15, a high fraction of deformation bands was observed with activation of second deformation products in the primary bands as shown in Fig. 8c. According to Sun et al. [32], the primary band would provide a modified orientation area, where secondary deformation products including secondary twins and SIM α″ were favored over continued deformation of the β matrix, resulting in a dense network of deformation bands. The feature shown in Fig. 8c depicts that with further plastic deformation, multiple deformation mechanisms, including secondary mechanical twins and SIM α″ were simultaneously operative, which was strongly correlated with multiplication of deformation bands. Fig. 8b and d show corresponding IPF maps of the ST3000 sample, indicating that a large fraction of undeformed area was still shown in individual grains. The observed primary band with ~100 μm in width was much thicker than that in the ST100 sample. Few secondary deformation bands were found in the microstructure at a strain of 0.15. This implies that the plastic deformation in the ST3000 sample was mainly accommodated by the

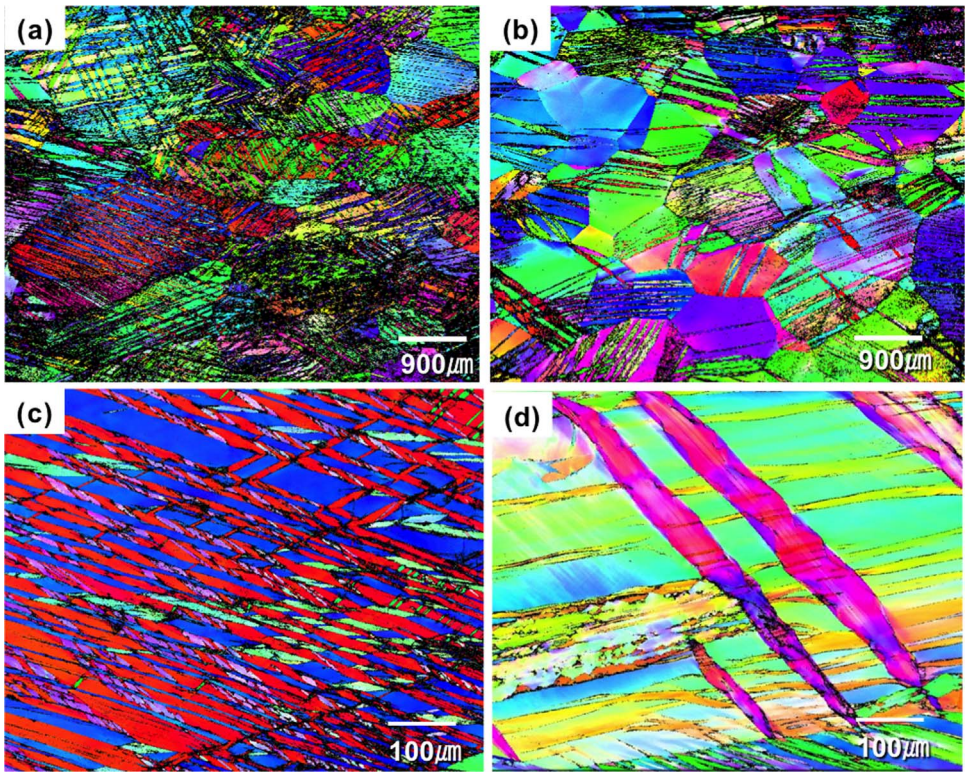

Fig. 8. IPF map of deformation structure in the specimen subject to cold rolling to 0.15 (a) and (c) ST100 and (b) and (d) ST3000.

primary bands being denser and thicker, rather than multiplication of the bands, as shown in Fig. 8d.

To further investigate the deformation band in Fig. 8d, detail EBSD was carried out with careful misorientation analysis. In the IPF map, the primary band shows slight different colors along its width as indicated by a line A to B in Fig. 9a. This illustrates that the crystallographic features were obviously different from each other, including crystallographic orientations or crystal structure, which might be a result of multiple phases. The KAM map (Fig. 9b) shows that the boundaries were clearly visualized in the primary band, which is attributed to different lattice distortions. Fig. 9c displays the misorientation profile of the line from A to B in Fig. 9a, indicates that the crystallographic misorientation between the β-matrix and the band was less than 20°, corresponding to SIM α″ phase. On the other hand, the point-to-point misorientation of the band along the distance between 58 μm and 112 μm were 59.7° and 59.2°, respectively, which correspond to the

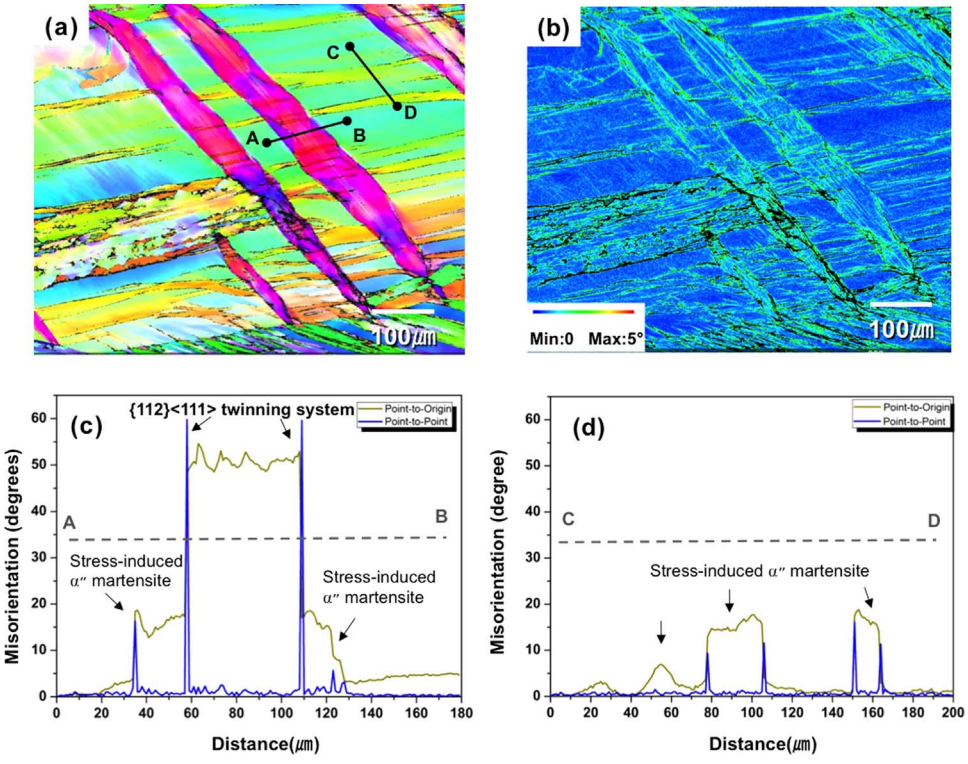

Fig. 9. EBSD analysis of deformation microstructure in the ST3000 (ε = 0.15): (a) IPF map, (b) KAM map, (c) and (d) Misorientation profiles relative to the first points along the arrows A-B (c) and C-D (d).

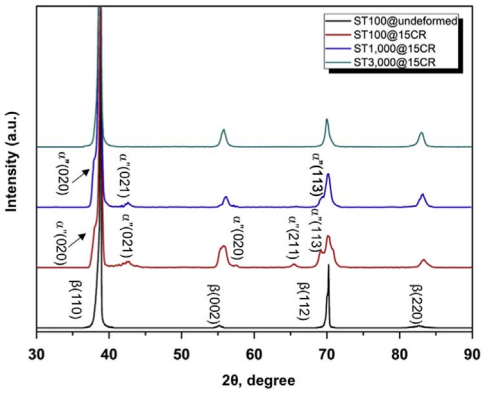

Fig. 10. XRD patterns of Ti-Nb-Ta-Zr-O alloys subject to solution treatment (ST100) and 15% cold rolling (ST100, ST1000, ST3000).

{112} < 111 > β twinning system as revealed in Section 3.3. The above results indicate that the deformation bands were characterized by SIM α" / {112} < 111 > β twin / SIM α″, in sequence. Fig. 9d corresponds to the misorientation profile of the bands as indicated by a line from C to D in Fig. 9a. It shows the crystallographic misorientation between β-matrix and the bands were less than 20°, illustrating that the bands were only composed of SIM α″ phase. This suggests that SIM α″ phase would be developed either at boundaries between the matrix and the primary twin or in the β-phase matrix, which might be a result of their orientation caused by high lattice distortion with accumulating strain [32]. Therefore, this demonstrates that the deformation bands were composed of both mechanical twins and SIM α″ or only SIM α″ phase in cold rolling to a strain of 0.15.

Fig. 10 shows XRD patterns of the ST100, ST1000 and ST3000 samples subject to cold-rolling (ε = 0.15) and solution-treated. Only the peaks of the β phase (body centered cubic, bcc) were indexed in the solution-treated ST100 sample, as shown in Fig. 10. It is worth noting that none of the ω phase, {thermally-induced martensitic transformation (β → ω)} during quenching [48], was detected in the three solution-treated samples, even though it has been previously observed in TEM analysis [53–56] in metastable Ti-Nb alloys. This may result from the nano-scale size and low volume fraction of the martensite phase, making it difficult to detect by conventional XRD analysis. With accumulating strain to 0.15, peaks corresponding to the α″ phase were observed in the ST100 and the ST1000 samples, both having a heterogeneous elemental distribution. This demonstrates the occurrence of the stress-induced martensitic transformation β → α″ in the heterogeneous specimens during plastic deformation. Comparing the intensity of α″ phase peaks between the cold rolled ST100 and ST1000 samples, higher intensity and more evident α″ peaks were indexed in the ST100 specimen. This might be due to a higher volume fraction of α″ phase in the ST100 sample, resulting from the enhancement of the SIM transformation with increasing cold deformation. On the other hand, no orthorhombic α″ peaks were found in the ST 3000 sample, even though SIM α″ was identified in microstructures deformed to 15%, as shown in Fig. 9. This might be due to fact that a negligibly amount of SIM α″ formed in a homogenized sample compared to that in a heterogeneous sample. Therefore, this illustrates that the fraction of deformation bands has a significant influence on the phase constitution of the alloys.

3.6. Influence of β-phase stability on hardness and elastic modulus

In order to establish the dependence of mechanical properties and elastic properties on the β-phase stability, as well as confirm the effect of plastic deformation on these properties, hardness and elastic modulus were measured by Vickers hardness and acoustic wave method, respectively. Fig. 11a shows the variation of microhardness of three specimens strained from 0 to 0.15, indicating that the hardness in three specimens increases slightly with accumulated strain, regardless of structural state (β-phase stability), with only about 8% increase in hardness with a cold-rolling reduction to 15%. This suggests that the alloys would show a relatively low work hardening behavior compared to conventional β-Ti alloys, which is in agreement with previous studies [12,57]. According to other studies [12–15,58], little or no work hardening has been observed during over 90% cold-deformation in Ti-Nb based Gum metals, which was attributed to non-conventional dislocation-free deformation mechanisms. Based on these theoretical and experimentally results, it would appear that dislocation activity has little effect on the mechanical behavior of these alloys. In the ST3000 sample, the measured hardness values, at different strain levels, were significantly higher than that of the ST100 and ST1000 specimens. The analysis presented in Section 3.2 shows that the ST100 and ST1000 specimens possess in-homogenized structures having relatively large volume fractions of deformation bands composed of mechanically induced twins and SIM α″, as compared to samples with a homogenized structure (e.g., in the ST3000). As is mentioned in several other studies [6,7,30–34,58], strain-hardening processes are presumably linked to the occurrence of multiple deformation mechanisms in metastable β-Ti alloys, which may result from transformation-induced plasticity (TRIP) effect and twinning-induced plasticity (TWIP) effect. This means that the mechanical behavior of β-Ti alloys largely depend on the interaction between these different deformation mechanisms. Therefore, the enhancement of twinning deformation and/or SIM α″ for achieving better ductility can be expected in the heterogeneous specimens like the ST100 and ST1000 samples. In addition, Hao et al. [59] suggested that SIM α″ possesses a lower hardness compared with the β-phase, which is well supported by the results of XRD analysis and hardness measurement in this study. As shown in Fig. 10, a relatively high volume fraction of SIM α″ phase was observed in the ST100 and ST1000, which can result in lower hardness values compared to that of ST3000. Therefore, these observations suggest that the deformation mechanism activated during plastic deformation has a significant effect on the mechanical properties in these alloys, which can be manipulated by the extent of β-phase stability, as discussed in Section 3.1.

Fig. 11b shows the elastic moduli of the three specimens subjected to solution treatment and cold rolling to 15%. The data reveals that the elastic modulus in all specimens decreased gradually with accumulating deformation to 15%, from 109 GPa to 91 GPa in the ST100 sample, from 96 GPa to 78 GPa in the ST1000 sample, and from 98 GPa to 76 GPa in the ST3000 sample which is in good agreement with the typical mechanical behavior of Ti-Nb Gum metal [13,14]. Furuta *et al.* [14] has reported that the elastic modulus of Gum Metals decreases with increasing cold working to 90% due to its highly textured microstructure (strong < 110 > texture) and/or a significant amount of stored elastic energy after deformation. In addition, ω-precipitates in solution treated alloys gradually disappear within the primary deformation band in the early stages of strain. Lai *et al.* [15] reported that the initiation and propagation of the deformation band leads to the deformation-induced transformation from ω-phase to β-phase, which is shown to lead to the formation of the channel depleted of athermal ω-phase. However, the mechanism for cold-deformed Gum Metal is still under discussion. Although the trend in elastic modulus with accumulated cold-deformation is similar to the trends observed for typical Gum Metals, the ST100 shows the highest elastic modulus of these three specimens. It is worth noting that the elastic modulus in metastable β-Ti alloys is highly dependent on the constituent phases of the alloy, resulting from the clear differences in elastic modulus of individual phases [59–61], and found to be related by the following approximations: $E_{\omega} \approx 2.0E_{\beta}$ and $E_{\alpha''} \approx E_{\beta}$ [59,62]. Therefore, it is important to clarify that as the volume fraction of the athermal ω-phase increases in the microstructure, the elastic modulus of the alloy would be increased (α″ phase has little effect on the elastic modulus of the β-phase Ti alloys [59]). As shown in Section 3.1, the ST100 specimen has the most heterogeneous elemental distribution and the least β-phase stability, being

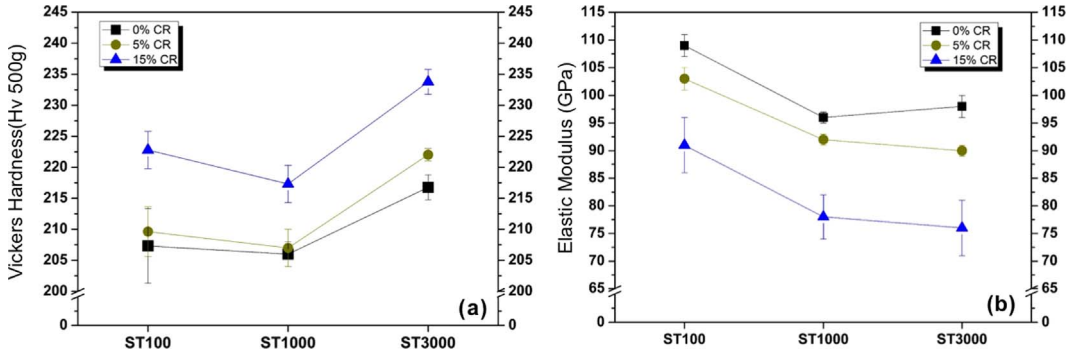

Fig. 11. (a) Micro-hardness and (b) Elastic modulus of Ti-Nb-Ta-Zr-O alloys (ST100, ST1000, ST3000) subject to solution treatment and cold-rolling to strains of 0.05 and 0.15.

located under the Ms transition line. By comparison, the more homogeneous specimens, ST1000 and ST3000, relatively few points representing the β-phase stability were observed under the Ms transition line. This implies that in more stable β-Ti alloys, the appearance of ω-phase was limited or absent, which results in lower elastic modulus of as-solution treated alloys. Although the volume fraction of the ω-phase in each alloy cannot be obtained quantitatively with our XRD analysis, due to its small fraction and size in the nanoscale, the formation or presence of athermal ω-phase in the three alloys is associated with both the chemical stability of the alloy and its deformation behavior. Furthermore, the ST1000 and ST3000 exhibit similar values of elastic modulus even with strain to level of 15%. It should be noted that between the ST1000 and ST3000, significantly different β-phase stability and mechanical behavior were characterized as can be observed in Fig. 4 and Fig. 11b. These results lead to a very important conclusion, that mechanical properties of the alloys can be controlled without elastic properties variation in the same chemical composition of Ti-Nb Gum Metal.

4. Summary

1. For the solution treated Ti-23Nb-0.7Ta-2Zr-0.8O (at%) alloy, the extent of β-phase stability was dependent on elemental distributions, which was controlled by the solution treatment process.
2. The effect of β-phase stability on the deformation behavior of the alloy was related to the deformation mechanism and could be described on the basis of characterization of deformation band at the initial stage of strain. In the ST3000 specimen, a fully homogenized structure, only mechanically-induced $\{332\}<113>_{\beta}$ twinning was observed, whereas in both the ST100 and ST1000 samples, having heterogeneous structures, were accompanied by multiple deformation mechanisms operative, including $\{112\}<111>_{\beta}$ twinning, $\{332\}<113>_{\beta}$ twinning and stress-induced α″ martensite during the early stages of deformation.
3. The preferential activation of the deformation mode was highly dependent on the chemical stability of the β-phase during an early stage of deformation, which plays a significant role in determining deformation behavior and constitute phase of the alloy.
4. β-phase stability plays an important role in determining the mechanical properties and the elastic properties of metastable Ti-alloys. The microhardness results revealed that the enhancement of the twinning deformation (TRIP) and/or SIM α″ (TRIP) for achieving better ductility can be expected in the heterogeneous specimens or homogeneous samples slightly off the current composition. It was also found that the elastic modulus of the alloys decreased with accumulating strain, which was highly dependent on phase constitution before and after cold working.

Acknowledgements

The authors would like to thank C. Zhu, T. Harrington, and H. Wang, University of California, San Diego, for their helpful suggestions, stimulating discussions and constant encouragement.

References

[1] D. Banerjee, J.C. Williams, Perspective on titanium science and technology, Acta Mater. 61 (2013) 844–879.
[2] M. Long, H.J. Rack, Titanium alloys in total joint replacement- A materials science perspective, Biomaterials 19 (1998) 1621–1639.
[3] S. Miyazaki, H.Y. Kim, H. Hosoda, Development and characterization of Ni-free Ti-base shape memory and superelastic alloys, Mater. Sci. Eng. A 438–440 (2006) 18–24.
[4] Y.L. Hao, S.J. Li, S.Y. Sun, R. Yang, Effect of Zr and Sn on Young's modulus and superelasticity of Ti–Nb-based alloys, Mater. Sci. Eng. A 441 (2006) 112–118.
[5] D.H. Ping, C.Y. Cui, F.X. Yin, Y. Yamabe-Mitarai, TEM investigations on martensite in a Ti–Nb-based shape memory alloy, Scr. Mater. 54 (2006) 112–118.
[6] X. Min, X. Chen, S. Emura, K. Tsuchiya, Mechanism of twinning-induced plasticity in β-type Ti–15Mo alloy, Scr. Mater. 69 (2013) 393–396.
[7] F. Sun, J.Y. Zhang, M. Marteleur, C. Brozek, E.F. Rauch, M. Veron, P. Vermaut, P.J. Jacques, F. Prima, A new titanium alloy with a combination of high strength, high strain hardening and improved ductility, Scr. Mater. 94 (2015) 17–20.
[8] P. John, S. Buenconsejo, H.Y. Kim, S. Miyazaki, Effect of ternary alloying elements on the shape memory behavior of Ti–Ta alloys, Acta Mater. 57 (2009) 2509–2515.
[9] S. Hanada, O. Izumi, Correlation of tensile properties, deformation modes, and phase stability in commercial b-phase titanium alloys, Metall. Trans. A 18 (1987) 265–271.
[10] M. Ahmed, D. Wexler, G. Casillas, O.M. Ivasishin, E.V. Pereloma, The influence of β phase stability on deformation mode and compressive mechanical properties of Ti-10V-3Fe-3Al alloy, Acta Mater. 84 (2015) 124–135.
[11] Y.L. Hao, S.J. Li, B.B. Sun, M.L. Sui, R. Yang, Ductile titanium alloy with low Poisson's ratio, Phys. Rev. Lett. 98 (2007) 216450.
[12] T. Saito, T. Furuta, J.-H. Hwang, S. Kuramoto, K. Nishino, N. Suzuki, R. Chen, A. Yamada, K. Ito, Y. Seno, T. Nonaka, H. Ikehata, N. Nagasako, C. Iwamoto, Y. Ikuhara, T. Sakuma, Multifuctional alloys obtained via a dislocation-free plastic deformation mechanism, Science 300 (2003) 464–467.
[13] J. Hwang, S. Kuramoto, T. Furuta, K. Nishino, T. Saito, Phase-stability dependence of plastic deformation behavior in Ti-Nb-Ta-Zr-O alloys, J. Mater. Eng. Perform. 14 (2005) 747–754.
[14] T. Furuta, K. Nishino, J.H. Hwang, A. Yamada, K. Ito, S. Osawa, S. Kuramoto, N. Suzuki, R. Chen, T. Saito, Development of multi functional titanium alloy, "Gum Metal", Ti-2003 science and technology, in: G. Lutjering, J. Albrecht, (Ed.) Proceedings of 10th World Conference on Titanium, Jul 13-18, 2003, Wiley, Hamburg, 2004, p 1519–1526.
[15] M.J. Lai, C.C. Tasan, D. Raabe, Deformation mechanism of ω-enriched Ti-Nb-based gum metal: dislocation channeling and deformation induced ω-β transformation, Acta Mater. 100 (2015) 290–300.
[16] Y. Yang, G.P. Li, G.M. Cheng, Y.L. Li, K. Yang, Multiple deformation mechanisms of Ti-22.4Nb-0.73Ta-2.0Zr-1.34O alloy, Appl. Phys. Lett. 94 (2009) 061901.
[17] Y. Yang, G.P. Li, G.M. Cheng, H. Wang, M. Zhang, F. Xu, K. Yang, Stress-introduced α″ martensite and twinning in a multifunctional titanium alloy, Scr. Mater. 58 (2008) 9–12.
[18] P. Castany, M. Besse, T. Gloriant, Dislocation mobility in gum metal β-titanium alloy studied via in situ transmission electron microscopy, Phys. Lett. B 84 (2011) 020201.
[19] E. Withey, M. Jin, A. Minor, S. Kuramoto, D.C. Chrzan, J.W. Morris Jr., The deformation of "gum metal" in nanoindentation, Mater. Sci. Eng. A 493 (2008) 26–32.
[20] M.Y. Gutkin, T. Ishizaki, S. Kuramoto, I.A. Ovid'ko, N.V. Skiba, Giant faults in deformed gum metal, Int. J. Plast. 24 (2008) 1333–1359.
[21] M.Y. Gutkin, T. Ishizaki, S. Kuramoto, I.A. Ovid'ko, Nanodisturbances in deformed gum metal, Acta Mater. 54 (2006) 2489–2499.
[22] R.J. Talling, R.J. Dashwood, M. Jackson, D. Dye, On the mechanism of superelasticity in Gum metal, Acta Mater. 57 (2009) 1188–1198.
[23] S. Kuramoto, T. Fruta, J.H. Hwang, K. Nishino, T. Saito, Plastic deformation in a multifunctional Ti-Nb-Ta-Zr-O alloy, Metall. Mater. Trans. A 37A (2006) 657–662.
[24] Y. Yang, S.Q. Wu, G.P. Li, Y.L. Li, Y.F. Lu, K. Yang, P. Ge, Evolution of deformation

mechanisms of Ti-22.4Nb-0.73Ta-2Zr-1.34O alloy during strain, Acta Mater. 58 (2010) 2778–2787.
[25] H. Xing, J. Sun, Q. Yao, W.Y. Guo, R. Chen, Origin of substantial plastic deformation in gum metals, Appl. Phys. Lett. 92 (2008) 151905.
[26] M. Besse, P. Castany, T. Gloriant, Mechanisms of deformation in gum metal TNTZ-O and TNTZ titanium alloys: a comparative study on the oxygen influence, Acta Mater. 59 (2011) 5982–5988.
[27] P. Castany, M. Besse, T. Gloriant, Dislocation mobility in gum metal β-titanium alloy studied via in situ transmission electron microscopy, Phys. Rev. B 84 (2011) 020201.
[28] T. Grosdidier, C. Roubaud, M.J. Philippe, Y. Combres, The deformation mechanisms in the β-metastable β-Cez titanium alloy, Scr. Mater. 36 (1997) 21–28.
[29] T. Grosdidier, M.J. Philippe, Deformation induced martensite and superelasticity in a β-metastable titanium alloy, Mater. Sci. Eng. A 291 (2000) 218–223.
[30] M. Marteleur, F. Sun, T. Gloriant, P. Vermaut, P.J. Jacques, F. Prima, On the design of new β-metastable titanium alloys with improved work hardening rate thanks to simultaneous TRIP and TWIP effects, Scr. Mater. 66 (2012) 749–752.
[31] D. Kuroda, M. Niinomi, M. Morinaga, Y. Kato, T. Yashiro, Design and mechanical properties of new β type titanium alloys for implant materials, Mater. Sci. Eng. A 243 (1998) 244–249.
[32] F. Sun, J.Y. Zhang, M. Marteleur, T. Gloriant, P. Vermaut, D. Laille, P. Castany, C. Curfs, P.J. Jacques, F. Prima, Investigation of early stage deformation mechanisms in a metastable β titanium alloy showing combined twinning induced plasticity and transformation-induced plasticity effects, Acta Mater. 61 (2013) 6406–6417.
[33] F. Sun, J.Y. Zhang, M. Marteleur, C. Brozek, E.F. Rauch, M. Veron, P. Vermaut, P.J. Jacques, F. Prima, A new titanium alloy with a combination of high strength, high strain hardening and improved ductility, Scr. Mater. 94 (2015) 17–20.
[34] X.H. Min, K. Tsuzaki, S. Emura, K. Tsuchiya, Enhancement of uniform elongation in high strength Ti-Mo based alloys by combination of deformation modes, Mater. Sci. Eng. A 528 (2011) 4569–4578.
[35] M. Morinaga, N. Yukawa, T. Maya, K. Sone, H. Adachi, Theoretical design of titanium alloys, in: Presented at the Sixth World Conference on Titanium Alloys, Cannes, France, 1988.
[36] M. Abdel-Hady, K. Hinoshita, M. Morinaga, General approach to phase stability and elastic properties of β-type Ti-alloys using electronic parameters, Scr. Mater. 55 (2006) 477–480.
[37] X. Zhao, M. Niinomi, M. Nakai, J. Hieda, T. Ishimoto, T. Nakano, Optimization of Cr content of metastable b-type TieCr alloys with changeable young's modulus for spinal fixation applications, Acta Biomater. 8 (2012) 2392–2400.
[38] T. Inamura, J.I. Kim, H.Y. Kim, H. Hosoda, K. Wakashima, S. Miyazaki, Composition dependent crystallography of α″-martensite in Ti-Nb-based β titanium alloy, Philos. Mag. 87 (2007) 3325–3350.
[39] W. Xu, K.B. Kim, J. Das, M. Calin, J. Eckert, Phase stability and its effect on the deformation behavior of Ti-Nb-Ta-in/Cr β alloys, Scr. Mater. 54 (2006) 1943–1948.
[40] M. Morinaga, N. Yukawa, H. Adachi, Electronic structure and phase stability of titanium alloys, Tetsu- to- Hagane 72 (1986) 555–562.
[41] Y. Yang, G.P. Li, H. Wang, S.Q. Wu, L.C. Zhang, Y.L. Li, K. Yang, Formation of zigzag-shaped {112} < 111 > mechanical twins in Ti–24.5 Nb–0.7 Ta–2 Zr–1.4 O alloy, Scr. Mater. 66 (2012) 211–214.
[42] T. Furuta, S. Kuramoto, J.H. Hwang, K. Nishino, T. Saito, Elastic deformation behavior of multi-functional Ti-Nb-Ta-Zr-O alloys, Mater. Trans. 46 (2005) 3001–3007.
[43] X.H. Min, K. Tsuzaki, S. Emura, K. Tsuchya, Heterogeneous twin formation and its effect on tensile properties in Ti-Mo based β titanium alloys, Mater. Sci. Eng. A 554 (2012) 53–60.
[44] H. Zhan, W. Zeng, G. Wang, D. Kent, M. Darusch, On the deformation mechanisms and strain rate sensitivity of a metastable β Ti-Nb alloy, Scr. Mater. 107 (2015) 34–37.
[45] E. Bertrand, P. Castany, I. Péron, T. Gloriant, Twinning system selection in a metastable β-titanium alloy by Schmid factor analysis, Scr. Mater. 64 (2011) 1110–1113.
[46] M. Calcagnotto, D. Ponge, E. Demir, D. Raabe, Orientation gradients and geometrically necessary dislocations in ultrafine grained dual-phase steels studied by 2D and 3D EBSD, Mater. Sci. Eng. A 527 (2010) 2738–2746.
[47] S.I. Wright, M.M. Nowell, D.P. Field, A review of strain analysis using electron backscatter diffraction, Microsc. Microanal. 17 (2011) 316–329.
[48] M.J. Lai, C.C. Tasan, D. Raabe, On the mechanism of {332} twinning in metastable β titanium alloys, Acta Mater. 111 (2016) 173–186.
[49] A. Bhattacharjee, S. Bhargava, V.K. Varma, S.V. Kamat, A.K. Gogia, Effect of β grain size on stress induced martensitic transformation in β solution treated Ti–10V–2Fe–3Al alloy, Scr. Mater. 53 (2005) 195–200.
[50] F.J. Gil, J.A. Planell, Behaviour of normal grain growth kinetics in single phase titanium and titanium alloys, Mater. Sci. Eng. A 283 (2000) 17–24.
[51] J.P. Liu, Y.D. Wang, Y.L. Hao, Y. Wang, Z.H. Nie, D. Wang, Y. Ren, Z.P. Lu, J. Wang, H. Wang, X. Hui, N. Lu, M.J. Kim, R. Yang, New intrinsic mechanism on gum-like superelasticity of multifunctional alloys, Sci. Rep. 3 (2013) 2156.
[52] H. Zhan, G. Wang, D. Kent, M. Dargusch, The dynamic response of a metastable β Ti-Nb alloy to high strain rates at room end elevated temperature, Acta Mater. 105 (2016) 104–111.
[53] Yano, Y. Murakami, D. Shindo, Y. Hayasaka, S. Kuramoto, Transmission electron microscopy studies on nanometer-sized ω phase produced in gum metal, Scr. Mater. 63 (2010) 536–539.
[54] M. Tane, T. Nakano, S. Kuramoto, M. Hara, M. Niinomi, N. Takesue, T. Yano, H. Nakajima, Low Young's modulus in Ti–Nb–Ta–Zr–O alloys: cold working and oxygen effects, Acta Mater. 59 (2011) 6975–6988.
[55] T. Yano, Y. Murakami, D. Shindo, S. Kuramoto, Study of the nanostructure of Gum Metal using energy-filtered transmission electron microscopy, Acta Mater. 57 (2009) 628–633.
[56] D. Doraiswamy, S. Ankem, The effect of grain size and stability on ambient temperature tensile and creep deformation in metastable beta titanium alloys, Acta Mater. 51 (2003) 167–1619.
[57] Y.F. Xu, D.Q. Yi, H.Q. Liu, X.Y. Wu, B. Wang, F.L. Yang, Effects of cold deformation on microstructure, texture evolution and mechanical properties of Ti–Nb–Ta–Zr–Fe alloy for biomedical applications, Mater. Sci. Eng. A 547 (2012) 64–71.
[58] C. Brozek, F. Sun, P. Vermaut, Y. Millet, A. Lenain, D. Embury, P.J. Jacques, F. Prima, A β-titanium alloy with extra high strain-hardening rate: design and mechanical properties, Scr. Mater. 114 (2006) 60–64.
[59] Y.L. Hao, M. Niinomi, D. Kuroda, K. Fukunaga, Y.L. Zhou, R. Yang, A. Suzuki, Young's modulus and mechanical properties of Ti-29Nb-13Ta-4.6Zr in relation to α″ martensite, Metall. Mater. Trans. A 33A (2002) 3137–3144.
[60] T. Li, J.W. Morris, N. Nagasako, S. Kuramoto, D.C. Chrzan, "Ideal" Engineering alloys, Phys. Rev. Lett. 98 (2007) 105503.
[61] M. Tane, S. Akita, T. Nakano, K. Hagihara, Y. Umakoshi, M. Niinomi, H. Nakajima, Peculiar elastic behavior of Ti–Nb–Ta–Zr single crystals, Acta Mater. 56 (2008) 2856–2863.
[62] Z. Fan, On the young's moduli of Ti-6Al-4V alloys, Scr. Mater. 29 (1993) 1427–1432.